# An Experimental Investigation of the Flow of Aqueous Non-Newtonian High Polymer Solutions Past a Sphere

**RAFFI M. TURIAN**

**University of Wisconsin, Madison, Wisconsin**

**The terminal velocities of spheres falling in aqueous solutions of hydroxyethyl cellulose and polyethylene oxide were determined with ruby and steel spheres. For each sphere the terminal velocity was obtained in seven cylinder sizes covering a range of sphere-to-cylinder diameter ratio from 0.0067 to 0.18. The data were used in an extrapolation to correct for the cylindrical wall effect. Several alternative extrapolation procedures for estimating the zero shear viscosity were attempted and the results were compared. An empirical correlation for the drag coefficient was developed in terms of the Ellis parameters of the fluids, and the Faxén wall correction for Newtonian flow. The correlation gives the drag coefficient within 4% for all cases in which the quantity $\eta_0 v_t/D\tau_{1/2}$ is less than 0.3.**

## NEWTONIAN FLOW PAST A SPHERE

The drag force exerted on a sphere of radius $R$ resulting from the flow past it of an unbounded incompressible Newtonian fluid of viscosity $\eta_0$ and approach velocity $v_\infty$ is given by Stokes' law (*12*):

$$F_S = 6\pi\eta_0 R v_\infty \tag{1}$$

Equation (1) is strictly valid in the so-called creeping flow region in which the Reynolds number, $N_{Re} = 2Rv_\infty\rho/\eta_0$, is less than about 0.1. Extensions of Stokes' solution to higher $N_{Re}$ have been presented by Oseen (*16*), by Goldstein (*7*), and by Proudman and Pearson (*17*). The drag force expression obtained by Proudman and Pearson is

$$F = 6\pi\eta_0 R v_\infty \left[ 1 + \frac{3}{16} N_{Re} + \frac{9}{160} N_{Re}^2 \ln\left(\frac{N_{Re}}{2}\right) + 0(N_{Re}^2) \right] \tag{2}$$

Oseen's approximation is represented by taking the terms up to and including $N_{Re}$ in Equation (2), whereas Goldstein's solution, purportedly an extension of Oseen's approximation, does not include the logarithmic term. These solutions are classified as the low Reynolds number flow approximations to the Navier-Stokes equations, and they possess certain interesting features, some of which have been discussed by Chester (*4*) (with regard to the Oseen approximation) and also by Proudman and Pearson (*17*).

Corrections to Stokes' equation to account for the effect of the cylindrical wall of the fluid container have been presented by Ladenburg (*11*) and by Faxén (*5*). Faxén's result, which extends the range of the correction to higher values of sphere-to-cylinder ratio $(D/D_c)$, and has been subjected to adequate experimental verification by Bacon (*1*), is

$$F = F_S/\left[ 1 - 2.104\left(\frac{D}{D_c}\right) + 2.09\left(\frac{D}{D_c}\right)^3 - 0.95\left(\frac{D}{D_c}\right)^5 + \dots \right] \tag{3}$$

According to Bacon the Faxén wall correction is valid up to $(D/D_c) = 0.32$. Ladenburg (*11*) has also presented a correction for the effect of the bottom of the cylinder. This correction, based on the solution for a sphere falling in an infinite fluid bounded at the bottom by an infinite flat plate, appears to overestimate the bottom correction. More recently, Tanner (*24*) carried out a numerical calculation in which the effects of both the cylindrical wall and the bottom of the container were taken into account. He found that the top and bottom corrections are negligible, provided the sphere is at least one cylinder radius away from either end. These conclusions are corroborated by experimental evidence and, consequently, the need for a top and bottom correction can be eliminated by appropriate design of the falling-sphere system.

Many other studies on the flow of Newtonian fluids past a sphere have been reported. These have been reviewed (*8, 13*) and will not be discussed inasmuch as the results are not employed in the present study.

## NON-NEWTONIAN FLOW PAST A SPHERE

Reported studies on non-Newtonian flow past a sphere include solutions based on perturbation procedures, solutions based on variational schemes, and empirical correlations and associated experimental studies.

### Solutions Based on Perturbation Procedures

A perturbation approximation for the flow of a Reiner-Rivlin-Prager fluid past a sphere was obtained by Rathna (*18*), who assumed that the viscosity and the cross viscosity are constant. The rheological model subject to these restrictions is inadequate in describing non-Newtonian behavior, and, moreover, the restriction of constant cross viscosity could, as indicated by Leigh (*14*), result in a flow which violates the second law of thermodynamics. Leslie (*15*) used the Oldroyd model for the rheological equation of the fluid. The main drawback in this result is that the Oldroyd model fails to give a sufficiently quantitative description of non-Newtonian behavior, although it does describe non-Newtonian, normal stress, and other effects qualitatively. Caswell and Schwarz (*3*) presented the perturbation approximation for the Rivlin-Ericksen fluid. These authors obtained what might be termed the equivalent of the Oseen solution for a Rivlin-Ericksen fluid. The material constants in this rheological model cannot be determined by viscometric data alone, and this

Raffi M. Turian is at Syracuse University, Syracuse, New York.

solution has not yet been compared with experiment.

#### Solutions Based on Variational Procedures

Ziegenhagen et al. (*31*) obtained an approximation to the drag force for the slow flow of a truncated power series fluid. The rheological model used is, however, quite unrealistic. Tomita (*26*) obtained a first approximation to the drag force exerted on a sphere by a power law fluid, and Slattery (*21*) extended this result and also obtained the first approximation for the Sisko model. Both the power law and the Sisko models are inadequate in the region of low shear since they predict an infinite viscosity in the limit of zero shear. Wasserman and Slattery (*29*) used the minimum and its reciprocal maximum variational principles that had been proposed by Johnson (*9, 10*) to obtain lower and upper bounds for the drag coefficient for creeping power law flow past a sphere. Both the approximate solutions of Tomita (*26*) and of Slattery (*21*) and also available experimental data of Slattery (*22*) fell outside these bounds. It is not known, however, whether the entirely unsatisfactory results of this comparison are due to the inadequacy of the rheological model or to the inadequacy of the experimental results, or, in fact, to both. Ziegenhagen (*32*) used a variational method together with numerical calculations to obtain the correction to the drag force due to the creeping flow of a Powell-Eyring fluid past a sphere. The Powell-Eyring model seems to describe the viscosity-shear rate behavior of a small class of fluids which exhibit non-Newtonian behavior at only moderately high shear. Falling sphere data on the few such fluids encountered in the experimental study carried out by Turian (*27*) indicate that the results for Newtonian flow are entirely adequate. Foster and Slattery (*6*) used a variational method to obtain the approximation to the drag force for the Reiner-Rivlin-Prager fluid with constant viscosity and cross viscosity. This is the same model used by Rathna (*18*) in his perturbation scheme, and the solution is therefore subject to the same objections, namely, that the model is inadequate and objectionable on the basis of the second law of thermodynamics.

#### Empirical Correlations and Associated Experimental Studies

Slattery (*22, 23*) correlated experimentally measured drag coefficients for aqueous sodium carboxymethyl cellulose (CMC) flow past spheres by means of the Ellis model. In obtaining his correlations Slattery assumed that the cylindrical wall effect is negligible. Tanner (*25*) obtained experimental falling-sphere data on a single fluid using three different cylinder diameters and found that the wall effect was important. This is also borne out by the results reported herein. Other studies include the recent empirical correlation by Valentik and Whitmore (*28*) on spheres falling in flocculated China clay suspensions which are known to behave like Bingham plastics possessing a yield stress.

## EXPERIMENTAL INVESTIGATION

For the experimental falling-sphere investigation reported here, aqueous solutions of commercial high molecular weight hydroxyethylcelluse (HEC) (Natrosol-250, type H, Hercules Powder Company) and polyethylene oxide (PEO) (Polyox WSR-301, Union Carbide) were used. The concentrations for the HEC solutions were 1.0 and 1.25% by weight and those for the PEO solutions were 1.0 and 2.0% by weight. Each of these four solutions was investigated at 20° and 30°C., in effect, resulting in eight non-Newtonian solutions.*

The falling-sphere apparatus used consisted of seven cylinders of different inside diameters, and of several sizes of ruby and steel spheres. Cylinder diameters and sphere densities and diameters are given in Table 1. The overall length of each cylinder was about 25.4 cm., and only about a 10-cm. section in the middle portion of each cylinder was used for determination of fall velocities. The fall distance for each cylinder was divided into two approximately equal (about 5 cm.) sections, and for each sphere the fall velocity was determined in the two sections to ensure attainment of terminal velocity. Cylinder diameters and fall distances were accurate to within less than 1%. All ruby spheres had a diameter tolerance of 0.00003 in. and a sphericity of 0.00001 in. The steel spheres were precision ball bearings with a diameter tolerance of 0.00001 in. All spheres were checked for uniformity of density by weighing batches containing different numbers of spheres of each size. The accuracy of the measured fall velocities varies depending upon the speed of the sphere, but is estimated to be within 4%, with most having accuracies within about 2%.

Table 1. Falling-Sphere Apparatus Used

| | |
|---|---|
| Cylinders: | |
| Diameters, cm.: | 1.74, 2.66, 3.69, 4.72, 5.32, 7.50, 9.51 |
| Overall length, cm.: | about 25.4 |
| Fall distances: | two 5-cm. sections |
| Spheres: | |
| Ruby sphere diameters, cm.: | 0.06350, 0.07620, 0.10000, 0.15875 |
| Ruby sphere density, g./cc.: | 3.980 |
| Steel sphere diameters, cm.: | 0.15875, 0.31750 |
| Steel sphere density, g./cc.: | 7.7943, 7.7552 |

The shear stress-shear rate dependence of each solution was determined with a cone-and-plate viscometer following the procedure recommended by Biery and Huppler (*2*). The estimated accuracy of these measurements is about 3%.

## THE CYLINDRICAL WALL CORRECTION

The measured terminal velocities can be corrected for the cylinder wall effect by extrapolation of plots of $v_t$ vs. $(1/D_c)$ to $(1/D_c) = 0$ for each sphere. Such a plot of the measured terminal velocities for solution 4, 1.0% aqueous HEC at 20°C., is shown in Figure 1. Plots for the other seven non-Newtonian solutions investigated were more or less similar to the one shown in Figure 1. For each sphere it was possible to draw straight lines through the data points to obtain the velocity $v_x$ corrected to infinite cylinder diameter. Examination of the $v_t$ vs. $1/D_c$ plots for the eight non-Newtonian solutions investigated revealed two important aspects of this type of flow. First, if the range of cylinder diameters used in an assessment of the wall effect is narrow, then it is entirely possible that the wall effect may be obscured by the usual experimental scatter of the data. This appears to be why Slattery (*22, 23*), using three cylinder diameters (4, 5, and 6 in.), concluded that the wall effect was unimportant. On the other hand, in the present investigation the range of cylinder diameters was 1.74 cm. $\leq D_c \leq$ 9.51 cm., and the measured terminal velocities show a definite discernible trend with cylinder diameter. Second, the relationship between $(v_t/v_x)$ and $(D/D_c)$ was found to be of the following type:

$$v_t/v_x = 1 - A(D/D_c) \qquad (4)$$

The coefficient $A$ depends on the particular non-Newtonian solution and also on the particular sphere used. For solution 4, 1.0% aqueous HEC at 20°C., the fall velocities for all four ruby spheres could be described by Equation (4) with a maximum deviation of ± 1% with $A$ = 1.94, whereas the fall velocities for the two steel spheres were described with a maximum deviation of ± 2.8% with $A$ = 1.60. For all solutions investigated, the coefficient $A$ varied between the values of 1.15 and 2.35, and, moreover, the fit of the data was better when $A$ was cal-

* A complete listing of all experimental data relating to this work can be found in Appendix A of reference 27.

culated for each individual sphere. Over the range of sphere-to-cylinder diameter ratio investigated, $0.0067 \leq D/D_c \leq 0.182$, the Faxén wall correction can be adequately represented by the first two terms, that is, the third- and fifth-order terms in $(D/D_c)$ are negligible. Consequently, we compare the Faxén correction in the form $f_d = 1 - 2.104\ (D/D_c)$ with Equation (4). In general, the coefficient $A$ in Equation (4) was found to differ from the value 2.104 for all solutions and all spheres, and for any given solution the difference was larger as the sphere diameter and/or density was increased, that is, as non-Newtonian effects became relatively more important. However, the difference between Equation (4) and the Faxén wall correction can be made as small as desired by either choosing very small and light spheres so sphere velocities are very small or by maintaining the value of $(D/D_c)$ very small. In the former case, the value of $A$ seems to approach 2.104, whereas in the latter the wall correction itself becomes negligible. We conclude, therefore, that the unrestricted use of the Faxén wall correction with non-Newtonian fluids is inappropriate, and also that a definitive assessment of the possible existence of a wall effect requires the use of a wide range of cylinder diameters. Sato et al. (*20*), using a large number of steel spheres with a polybutadiene and a polyisoprene-toluene solution in several cylinder diameters, also found that the Faxén correction was inadequate under general conditions.

## EXTRAPOLATION PROCEDURES FOR THE ZERO-SHEAR VISCOSITY

In this section we compare values of the zero shear viscosity $\eta_0$ obtained by several extrapolation procedures. Because falling-sphere data are usually taken in a single cylinder diameter, whereby the Faxén wall correction must be used, the comparisons presented here will include procedures which utilize the Faxén correction also. Such a comparison will represent an additional test of the utility and limitations of the Faxén correction.

### Extrapolation of ln $\eta_s$ vs. $(\eta_s v_\infty/D)$ to $(\eta_s v_\infty/D) = 0$

In terms of the velocities $v_\infty$ corrected for the wall effect by extrapolation to $1/D_c = 0$, we define the quanti-

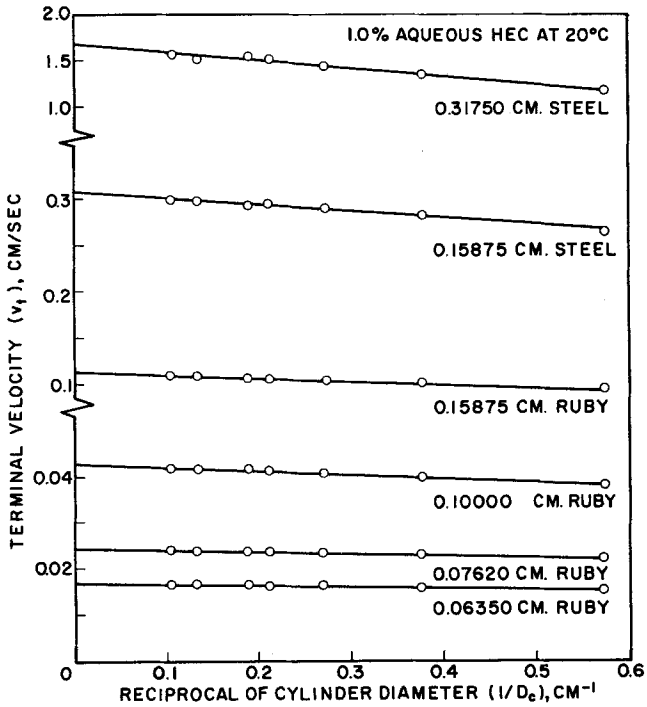


Fig. 1. Measured terminal velocity of sphere vs. reciprocal of cylinder diameter for 1.0% hydroxethyl cellulose in water.

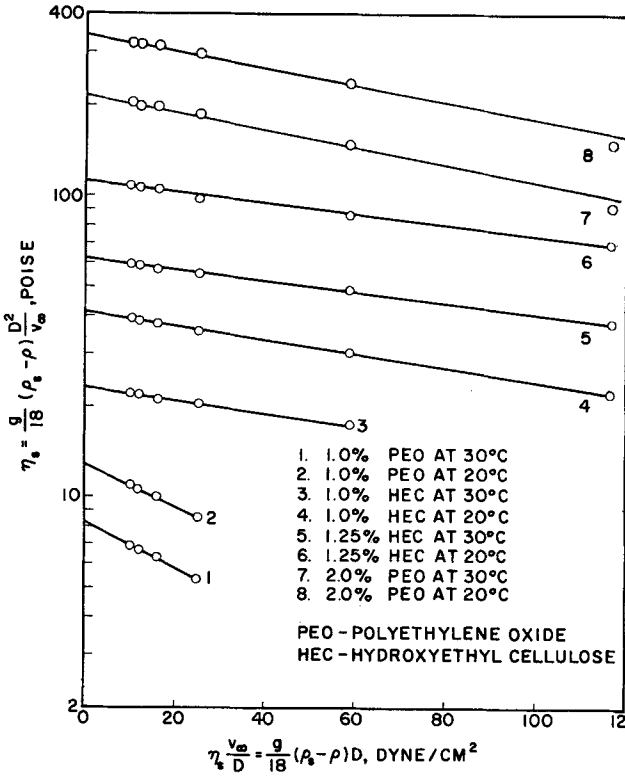


Fig. 2. $\eta_s = \dfrac{g}{18}(\rho_s-\rho)\dfrac{D^2}{v_\infty}$ as a function of the quantity $g(\rho_s-\rho)D/18$ for the sphere.

ties

$$\eta_s = \frac{g}{18}(\rho_s - \rho)\frac{D^2}{v_\infty} \tag{5}$$

and

$$\eta_s \frac{v_\infty}{D} = \frac{g}{18}(\rho_s - \rho)D \tag{6}$$

The quantities $\eta_s$ and $(\eta_s v_\infty/D)$ have units of viscosity and shear stress, respectively. For Newtonian fluids in creeping flow, the quantity $\eta_s$ would be the viscosity of the fluid as calculated from Stokes solution, while the quantity $(\eta_s v_\infty/D)$ is related to the square root of the maximum or average value over the sphere surface of the second invariant of the shear stress tensor, with suitable numerical coefficients in each case. For non-Newtonian fluids, on the other hand, these two quantities cannot be interpreted as the viscosity and corresponding shear stress. However, since they are experimentally determined independent variables, we plot ln $\eta_s$ vs. $(\eta_s v_\infty/D)$. These plots for all eight non-Newtonian solutions are shown in Figure 2. We note here that for the two least viscous fluids, solutions 1 and 2, accurate fall velocity data with the steel spheres could not be obtained, while for the next more viscous fluid, solution 3, only the smaller of the two steel spheres could be used. For all remaining solutions, however, all the ruby and steel spheres were used. It is clear from Figure 2 that the relation between $\eta_s$ and $(\eta_s v_\infty/D)$ is of the form

$$\log(\eta_0/\eta_s) = E(\eta_s v_\infty/D) \tag{7}$$

with $E$ a positive constant characteristic of the particular non-Newtonian solution, and $\eta_0$ the value of $\eta_s$ obtained by extrapolating the plots in Figure 2 to $(\eta_s v_\infty/D) = 0$. The values of $\eta_0$ for each solution obtained by this method of extrapolation are listed in column 1 of Table 2. These will be compared with $\eta_0$ values obtained by the other extrapolation procedures presented below. The magnitude of $E$ is a measure of how non-Newtonian the particular solution is. We observe that $E$ is larger for the polyethyl-

ene oxide solutions, 1, 2, 7 and 8, even though for solutions 7 and 8 the sphere velocities were lower than the corresponding ones for the remaining six solutions.

**Extrapolation Based on Analytical Solutions for Flow Past a Sphere**

The drag force for the creeping flow past a sphere of a Rivlin-Ericksen fluid of infinite extent is given by Caswell and Schwarz (3):

$$F = 3\pi D\eta_o v_\infty \left(1 + \frac{3}{16}\frac{D\rho v_\infty}{\eta_o}\right) + \frac{54\pi v_\infty^3}{D}$$
$$\left\{4.5278\left(1 + 2.4528\frac{\phi_2}{\phi_3}\right)\left(1 + \frac{\phi_2}{\phi_3}\right)\frac{\phi_3^2}{\eta_o}\right.$$
$$\left. + 3.0984(\phi_5 + \phi_6) - 5.6160\phi_4 - 1.0296\phi_5\right\} \quad (8)$$

In this equation $\eta_o$ is the zero shear viscosity and $\phi_i$ are material parameters, which, within the order of approximation involved in deriving this result, are constant for a given fluid. Consequently, we can take the coefficient of the term $(v_\infty^3/D)$ on the right-hand side as a constant. Furthermore, if we substitute the value $1/6\pi D^3(\rho_s - \rho)g$ for $F$, and divide the resulting equation by $3\pi Dv_\infty$, we get the expression for the quantity we have designated by $\eta_s$

$$\eta_s = \frac{g}{18}(\rho_s - \rho)\frac{D^2}{v_\infty} = \eta_o + \frac{3}{16}\rho Dv_\infty + C\frac{v_\infty^2}{D^2} \quad (9)$$

in which $C$ is a constant for a given fluid. From Equation (9) we note that, if falling-sphere data have been obtained at sufficiently low values of $v_\infty$ for the approximation to be valid, the plot of $\left(\eta_s - \frac{3}{16}\rho Dv_\infty\right)$ against $(v_\infty^2/D^2)$ should define straight lines which should intercept the $(v_\infty^2/D^2) = 0$ axes at $\eta_s = \eta_o$.

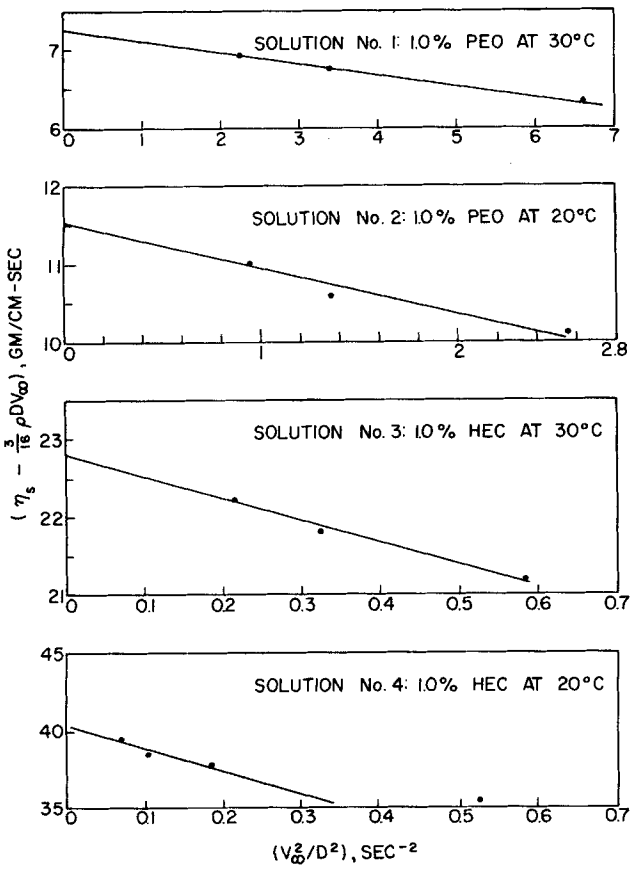


Fig. 3a. $\left(\eta_s - \frac{3}{16}\rho Dv_\infty\right)$ against $(v^2_\infty/D^2)$ for solutions 1 to 4.

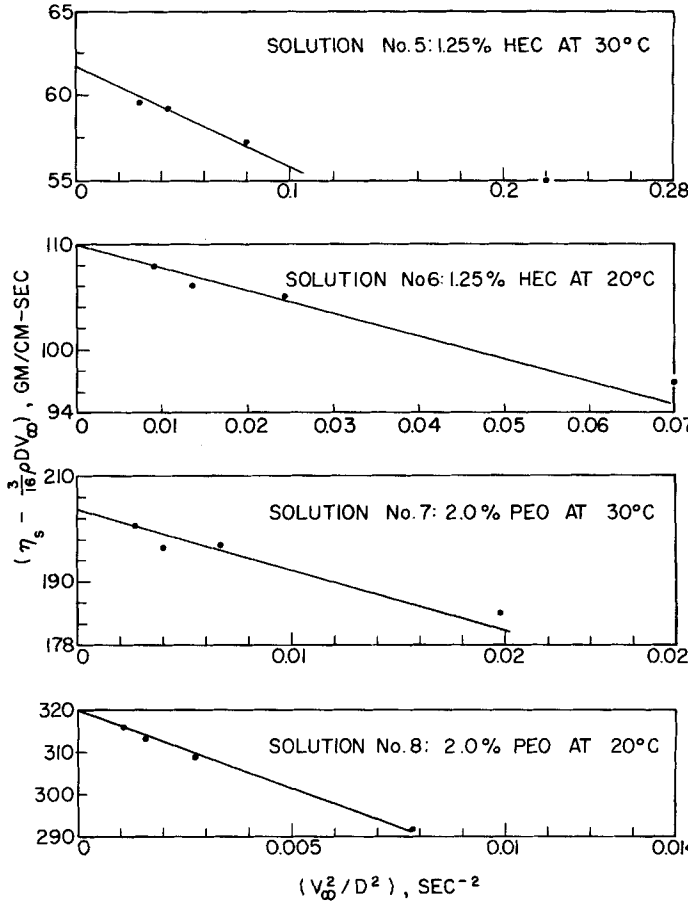


Fig. 3b. $\left(\eta_s - \frac{3}{16}\rho Dv_\infty\right)$ against $(v^2_\infty/D^2)$ for solutions 5 to 8.

We present in Figures 3*a* and 3*b* the plots of $\left(\eta_s - \frac{3}{16}\rho Dv_\infty\right)$ against $(v_\infty^2/D^2)$ for all eight solutions investigated. The values of $\eta_o$ obtained from these plots are given in column 2 of Table 2. A few remarks regarding the plots in Figures 3*a* and 3*b* are:

1. These plots do define straight lines for each of the eight solutions investigated. For solutions 1 through 5 the data for the three smallest ruby spheres are employed to define the straight lines, while for solutions 6 through 8 the data for the four smallest spheres (ruby) are employed.

2. None of the data points which are used to define the straight lines in Figures 3*a* and 3*b* deviates from the value at the straight line by more than the estimated experimental error of the data.

3. The computed Reynolds numbers $(D\rho v_\infty/\eta_o)$ for the data points used in defining the straight lines in Figures 3*a* and 3*b* ranged between a high of $3.5 \times 10^{-3}$ down to a low of $4.0 \times 10^{-7}$.

Comparison of the values of $\eta_o$ in column 2 of Table 2 with those of column 1 shows that there is rather close agreement, with the exception of the values for solutions 1 and 2 for which the relative difference is somewhat larger. One can attribute this difference, in part, to the fact that for these two least viscous solutions the falling-sphere data were of somewhat lower accuracy and, moreover, because of the smaller magnitude of the $\eta_o$ value, errors introduced by extrapolation will be relatively more

Table 2. Zero-Shear Viscosities Obtained by Extrapolation

| Solution | | | $\eta_0$, poise 1 | 2 | 3 | 4 |
|---|---|---|---|---|---|---|
| 1 | 1.0% | PEO at 30°C. | 8.37 | 7.25 | 7.95 | 8.29 |
| 2 | 1.0% | PEO at 20°C. | 13.0 | 11.5 | 12.7 | 13.3 |
| 3 | 1.0% | HEC at 30°C. | 23.2 | 22.8 | 23.3 | 23.4 |
| 4 | 1.0% | HEC at 20°C. | 41.4 | 40.6 | 41.4 | 41.8 |
| 5 | 1.25% | HEC at 30°C. | 62.0 | 61.5 | 62.6 | 63.6 |
| 6 | 1.25% | HEC at 20°C. | 113.0 | 110.0 | 113.6 | 113.4 |
| 7 | 2.0% | PEO at 30°C. | 212.0 | 204.0 | 210.4 | 210.2 |
| 8 | 2.0% | PEO at 20°C. | 332.0 | 320.0 | 329.4 | 331.3 |

1. Extrapolation of log $(\eta_s)$ vs. $(\eta_s v_x/D)$ to $(\eta_s v_\infty/D) = 0$.
2. Extrapolation of $(\eta_s - \frac{3}{16}\rho D v_x)$ vs. $(v_\infty^2/D^2)$ to $(v_\infty^2/D^2) = 0$.
3. Extrapolation of $\eta_s$ vs. $(D/D_c)$ to $(D/D_c) = 0$.
4. Extrapolation of log $(\eta_s' f_d)$ vs. $(\eta_s' v_t/D)$ to $(\eta_s' v_t/D) = 0$.

important. It might be added here that for the six data points used in defining the straight lines for solutions 1 and 2 the Reynolds numbers ranged between $3.5 \times 10^{-3}$ to $3.3 \times 10^{-4}$. The Reynolds numbers for the data points used in defining the straight lines for solutions 3 through 8, on the other hand, ranged between $3.4 \times 10^{-4}$ and $4.0 \times 10^{-7}$. Thus, the data points for solutions 1 and 2 correspond to a Reynolds number range which is higher than that for the data points for solutions 3 through 8.

Over a narrow range of shear stress near the value $\eta_o$, it seems reasonable to assume that the Rivlin-Ericksen model will describe the rheological behavior of the fluids investigated here. The fact that it is possible to obtain straight lines in Figures 3*a* and 3*b* is an indication that falling-sphere data at sufficiently low values of $v_x$ to estimate $\eta_o$ have been obtained in the present investigation. It should further be mentioned that one could have used Leslie's (*15*) expression for the drag force for the type of extrapolation carried out in this section, because his expression also contains a $(v_x^3/D)$ non-Newtonian contribution term to the drag force. This, despite the fact that Leslie's result does not contain the $(3/16)(D\rho v_\infty/\eta_o)$, Oseen correction term contained in the Caswell and Schwarz result. The magnitude of this term is negligibly small for all the data points shown in Figures 3*a* and 3*b*. Consequently, the comparison of experiment and theory presented in this section also shows that non-Newtonian effects become important at sphere velocities which are considerably lower than those for which inertial effects are also important. Perhaps this might also explain the relatively larger deviations of the extrapolated values of $\eta_o$ for solutions 1 and 2. Obviously, non-Newtonian effects place a more severe restriction on the range of applicability of Equation (8) than does the creeping flow restriction, at least for the non-Newtonian fluids under consideration here. Of course, the comparison presented here does not purport to be a test of the Rivlin-Ericksen model or the range of applicability of the result in Equation (8). A critical test of this sort must await the availability of data sufficient for an independent evaluation of the material constants in the equation. Nonetheless, the flow past a sphere itself represents an additional method for the determination of some of the rheological parameters themselves. This is important since the material parameters contained in Equation (8) cannot be determined independently from one-dimensional viscometric flow experiments alone.

### Extrapolation Procedures with the Faxen Wall Correction

It will be useful to determine the zero shear viscosities when the wall effect is accounted for by the Faxén correction, because most falling sphere data are taken in a single cylinder diameter whereby a procedure of this sort is inevitable. To describe the extrapolations in this section we define the quantities

$$\eta_s' = \frac{g}{18}(\rho_s - \rho)\frac{D^2}{v_t} \tag{10}$$

$$f_d = 1 - 2.104\left(\frac{D}{D_c}\right) + 2.09\left(\frac{D}{D_c}\right)^3 - 0.95\left(\frac{D}{D_c}\right)^5 \tag{11}$$

We note that $\eta_s'$ is defined in terms of the actual measured terminal velocity $v_t$, and $f_d$ is the Faxén wall correction.

In terms of $\eta_s'$ and $f_d$ defined by Equations (10) and (11), respectively, the following two extrapolation procedures are attempted for determining $\eta_o$:

1. Plot $(\eta_s' f_d)$ vs. $(D/D_c)$, extrapolate to $(D/D_c) = 0$, and average the extrapolated values for the different cylinder diameters to get $\eta_o$ (Figure 4 and column 3 in Table 2).
2. Plot log $(\eta_s' f_d)$ vs. $(\eta_s' v_t/D)$, and extrapolate to $(\eta_s' v_t/D) = 0$ to get $\eta_o$ (Figure 5 and column 4 in Table 2).

Extrapolation 1 is a linear plot of $(\eta_s' f_d)$ against $(D/D_c)$. Figure 4 represents such a plot for solution 4, 1.0% aqueous HEC at 20°C. Clearly, in such a plot there is a dependence on cylinder diameter. However, the values of the intercept at $(D/D_c) = 0$ for all solutions do not show any trend with cylinder diameter, and for any given solution the $\eta_o$ values obtained by extrapolating $(\eta_s' f_d)$ vs. $(D/D_c)$ to $(D/D_c) = 0$ for each cylinder diameter agreed with the average for all seven cylinders by well within the experimental accuracy of 3%. The values of $\eta_o$ listed in column 3 of Table 2 represent for each solution the average for seven cylinder diameters. Comparison of columns 1, 2, and 3 shows that there is rather close agreement in extrapolated values of $\eta_o$. The extrapolation in Figure 4 represents an essentially different procedure from the two previously discussed. The main disadvantage of the extrapolation procedure in Figure 4 is that it must be used with spheres of the same density. Therefore the plots in Figure 4 are only for the ruby spheres, the $(\eta_s' f_d)$ values for the steel spheres being smaller compared with those of the ruby spheres of the same $(D/D_c)$. Data were taken using only two steel sphere sizes; consequently, these cannot be used in this type of extrapolation, particularly since the smallest steel sphere diameter was equal to the largest ruby sphere diameter (1/16 in.) used.

The extrapolation of log $(\eta_s' f_d)$ against $(\eta_s' v_t/D)$ to $(\eta_s' v_t/D) = 0$ is shown in Figure 5 for solution 4. The

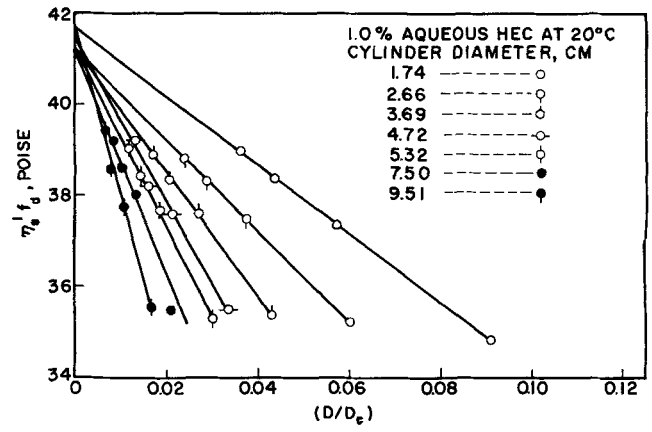


Fig. 4. $\eta_s f_d$ vs. $(D/D_c)$ for 1.0% hydroxyethyl cellulose. Only the data on ruby spheres are plotted.

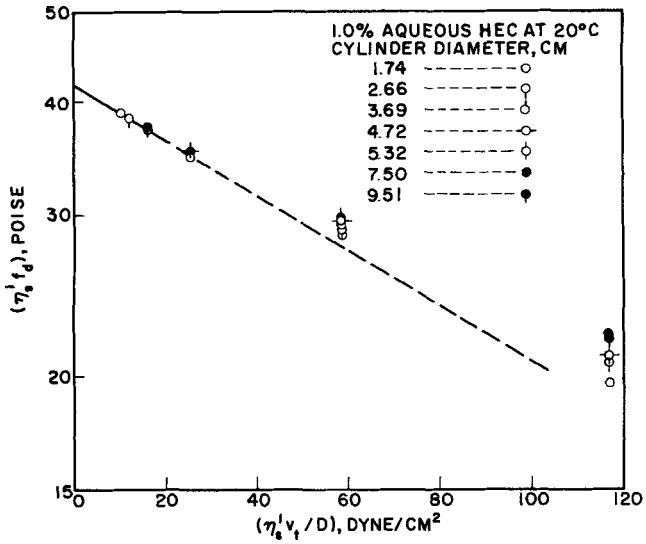


Fig. 5. log $(\eta_s f_d)$ vs. $(\eta_s v_t/D)$ for 1.0% hydroxyethyl cellulose. Plot consists of forty-two data points, many of which overlap for small $(\eta_s v_t/D)$.

essential difference between this plot and the one shown in Figure 2 is that in Figure 5 the wall correction is accomplished by means of the Faxén correction. The values of $(\eta_s v_\infty/D)$ and $(\eta_s' v_t/D)$ are the same, since they are both equal to $g/18\ (\rho_s - \rho)D$. However, the inadequacy of the Faxén correction as the value of $(\eta_s' v_t/D)$ becomes large is clearly shown in Figure 5. There are forty-two data points in Figure 5, but there is considerable overlap for the three smallest ruby spheres. In order to obtain $\eta_0$ by extrapolation of Figure 5 the data points corresponding to these three smallest spheres must be favored considerably more heavily than in Figure 2, where it is possible to incorporate the data on all of the spheres in the extrapolation. The $\eta_0$ values obtained by the extrapolation of Figure 5 are listed in column 4 of Table 2.

In concluding this section on extrapolation procedures, we note that the close agreement of the values of $\eta_0$ obtained by the different methods represented by Figures 2, 3*a*, 3*b*, and 4 indicates that the methods are sound and at least consistent. The extrapolations represented by Figures 4 and 5 represent also a test of the applicability of the Faxén wall correction. Obviously, the unrestricted use of this correction with non-Newtonian fluids is inappropriate. It seems to work relatively better as the ratio of sphere-to-cylinder diameter $(D/D_c)$ becomes very small where the correction itself becomes unimportant, and it also seems to work better in those regions of flow where non-Newtonian effects are small. This latter situation is generally attained with very small and low density spheres; the smallness of the spheres will depend on how strongly shear sensitive the rheological behavior is.

## CORRELATION FOR DRAG COEFFICIENT

An attempt was made to correlate the drag coefficients for flow past a sphere in terms of the Ellis model (*19*), which for one-dimensional flow is given by

$$\eta = \eta_0 / \left[1 + \left(\frac{\tau}{\tau_{1/2}}\right)^{\alpha-1}\right] \qquad (12)$$

in which $\eta$ and $\tau$ are the viscosity and the corresponding value of shear stress, and $\eta_0$, $\tau_{1/2}$ and $\alpha$ are model parameters. Defining a Reynolds number by $N_{Re} = (D\rho v_t/\eta_0)$, and a so-called Ellis number by $N_{El} = (\eta_0 v_t/D\tau_{1/2})$, one can show by dimensional reasoning that the drag coefficient, defined here by

$$f = F/\left(\frac{1}{4}\pi D^2 \cdot \frac{1}{2}\rho v_t\right)$$

is given by

$$f = f\left(N_{Re}, N_{El}, \alpha, \frac{D}{D_c}\right) = \frac{24}{N_{Re} f_d}$$
$$[1 + N_{El} g\ (N_{Re}, N_{El}, \alpha)] \qquad (13)$$

in which the second functional form utilizes the fact that an Ellis fluid attains Newtonian behavior when $N_{El} = 0$. It will be noticed that in Equation (13) we use the actual measured terminal velocities $v_t$, and account for the wall effect by inclusion of the Faxén correction $f_d$. This type of procedure fails to account for the interaction of wall and non-Newtonian effects which obviously exists especially at higher sphere velocities. The Ellis parameters were obtained by fitting the data from the cone-and-plate viscometer, which gives the dependence of $\eta$ on $\tau$ (Figure 6). However, the parameter $\eta_0$ was taken as the value tabulated in Table 2, column 4, because an arbitrary curve fitting of the cone-and-plate data to an empirical model, like the Ellis model, would not ensure that the $\eta_0$ parameter value is the zero shear viscosity, particularly since the lowest value of shear stress at which accurate viscometric data could be obtained with the cone-and-plate viscometer available for this investigation was about 65 dynes/sq.cm. With $\eta_0$ known Equation (12) can be rewritten in the form

$$\log\left(\frac{\eta_0}{\eta} - 1\right) = \log\left(\frac{\tau}{\tau_{1/2}}\right)^{\alpha-1} \qquad (14)$$

From a plot of $\log(\eta_0/\eta - 1)$ against $\log(\tau)$, the parameters $\tau_{1/2}$ and $\alpha$ can be obtained from straight lines drawn through the plots. However, since the Ellis model does not describe the viscometric data over an unrestricted range, the straight lines were drawn through the points in the lowest measured range of shear stresses. The Ellis parameters obtained by this procedure are given in Table 3, together with the range of shear stresses over which they apply.

A simple form of the relation for the drag coefficient is

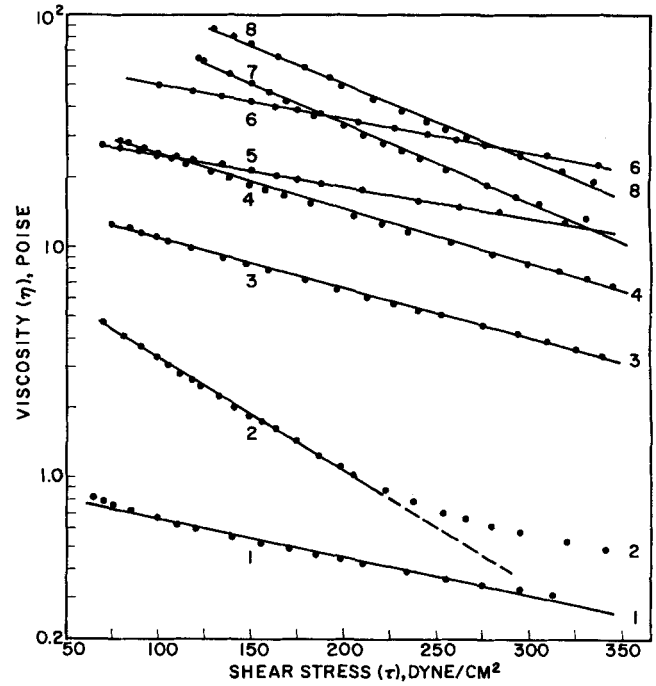


Fig. 6. Viscosity-shear stress dependence using the cone-and-plate viscometer. Solutions are identified in Figure 2.

Table 3. Ellis Parameters for High Polymer Solutions

| Solution | | | $\eta_o$ poise | $\tau_{1/2}$ dyne/sq.cm. | $\alpha$ | Range,* dyne/sq.cm. | Percent deviation Avg. | Max. |
|---|---|---|---|---|---|---|---|---|
| 1 | 1.0% | PEO at 30°C. | 8.29 | 5.04 | 1.788 | 87 to 1,000 | 3.2 | 10.1 |
| 2 | 1.0% | PEO at 20°C. | 13.3 | 48.3 | 2.566 | 70 to 175 | 2.6 | 8.7 |
| 3 | 1.0% | HEC at 30°C. | 23.4 | 88.5 | 2.079 | 75 to 230 | 2.7 | 9.8 |
| 4 | 1.0% | HEC at 20°C. | 41.8 | 131.0 | 2.627 | 80 to 392 | 1.7 | 7.4 |
| 5 | 1.25% | HEC at 30°C. | 63.6 | 39.2 | 1.475 | 65 to 190 | 2.6 | 8.9 |
| 6 | 1.25% | HEC at 20°C. | 113.4 | 75.3 | 1.775 | 100 to 275 | 3.0 | 10.0 |
| 7 | 2.0% | PEO at 30°C. | 210.3 | 77.3 | 2.788 | 120 to 310 | 2.5 | 9.5 |
| 8 | 2.0% | PEO at 20°C. | 331.3 | 72.0 | 2.690 | 130 to 240 | 2.3 | 7.6 |

* The lower limit of the range represents the lowest value which could be measured accurately on the cone-and-plate instrument used for this research.

$$f = \frac{24}{N_{Re} f_d} \{1 - A N_{Re}^B N_{El}^C (\alpha - 1)^N\} \qquad (15)$$

in which $A$, $B$, $C$, and $N$ are adjustable constants, and $f_d$ is the Faxén wall correction given in Equation (11). The quantities $N_{Re} = D\rho v_t/\eta_o$ and $N_{El} = \eta_o v_t/D\tau_{1/2}$ are defined in terms of the actual measured terminal velocity $v_t$. Usually this is the type of information available from experiments. The correction $f_d$ will be only adequate when non-Newtonian effects are small, that is, $N_{El}$ is small.

The constants $A$, $B$, $C$, and $N$ were determined, using 301 experimental falling-sphere data, by linear regression of the following form of Equation (15):

$$\ln\left\{1 - \frac{f f_d N_{Re}}{24}\right\} = \ln A + B \ln N_{Re} + C \ln N_{El} + N \ln(\alpha - 1) \qquad (16)$$

When the adjusted values of the constants are substituted into Equation (15), we get the correlation

$$f = \frac{24}{N_{Re} f_d} \{1 - 0.528 N_{Re}^{0.112} N_{El}^{0.417} (\alpha - 1)^{0.571}\} \qquad (17)$$

The drag coefficients calculated with Equation (17) were compared with those calculated from the experimental data with $f = [4g(\rho_s - \rho)D]/3\rho v_t^2$. The two values agreed within about 4% for $N_{El} \leq 0.3$. Even though the value $N_{El}$ was larger than 0.3 for 149 out of the 301 data points, the correlation (17) was obtained with all 301 data. The value $N_{El}$ was larger than 0.3 for all steel spheres and for the ruby spheres for the two least viscous solutions 1 and 2. Not surprisingly, these were precisely the data which showed the largest deviation from the Faxén wall correction. For these data the non-Newtonian effects are larger and the deviation can be attributed to the inability of the Faxén correction to account for the interaction of non-Newtonian and wall effects.

In addition, the Ellis model is only able to describe the present viscometric data over a rather narrow range of the measured shear stress. It must be emphasized that in obtaining the Ellis parameters, we deliberately chose $\eta_o$ to be the same as the value obtained from extrapolation of the falling-sphere data. The use of other criteria, such as, for example, obtaining all three Ellis parameters by curve fitting the cone-and-plate data over the widest possible measured range of shear, would not necessarily ensure that the parameter value $\eta_o$ thus obtained is the zero shear viscosity. All one can say about such a value is that it describes the viscometric data over precisely the range of shear used to obtain the parameters themselves. Obviously, then, the choice of the parameter $\eta_o$ in the Ellis model is arbitrary and it is often, in fact, possible to have different values of $\eta_o$ describing the same viscometric data equally adequately over the same range of shear, the differences in $\eta_o$ values being compensated for by appropriate adjustment of the remaining model parameters $\tau_{1/2}$, and $\alpha$. This is particularly obvious with viscometric data which are in the power law range, since then the parameter $\eta_o$ is really redundant. Our choice of $\eta_o$ as the value obtained from extrapolation of the falling-sphere data therefore seems appropriate. Unfortunately, the Ellis model does not seem to describe the viscometric data for the eight non-Newtonian solutions under consideration here over a sufficiently wide range of shear to warrant extensions of the correlation (17) to higher values of $N_{El}$.

## SUMMARY AND CONCLUSIONS

The experimental data on which this report is based were taken with two polymer species, hydroxyethyl cellulose and polyethylene oxide, with two concentrations for each polymer and with each solution tested at two different temperatures. The falling-sphere apparatus used consisted of four sizes of precision ruby spheres ranging in diameter from 0.025 in. to 1/16 in. and two sizes of precision steel spheres with diameters of 1/16 and 1/8 in. The terminal velocity of each sphere was determined in seven cylinders ranging in diameter from 1.74 to 9.51 cm., and in each case the velocity was determined in two consecutive sections of the fall distance to ensure attainment of terminal velocity and to assess the possible presence of a cylinder bottom effect. The range of sphere velocities encountered in this investigation was from $1.92 \times 10^{-3}$ to 1.57 cm./sec., with 301 different data within this range, while the range of sphere-to-cylinder diameter ratio was varied between 0.0067 and 0.182 with thirty-five different values of $D/D_c$ within this range.

The following conclusions are made from this investigation:

1. To ensure the detection of a discernible trend between sphere velocity and cylinder diameter, a wide range in cylinder diameters must be used. Otherwise, the wall effect could be obscured by the usual experimental scatter of the data.

2. Corrections for the cylinder top and bottom are unnecessary provided the section used for velocity determinations is at least a distance of one cylinder radius from either end of the cylinder for Newtonian fluids (*24*) and perhaps, as a safeguard, a slightly larger distance for non-Newtonian fluids. The use of the Ladenburg (*11*) bottom correction, derived for a different geometry, with spheres falling in cylinders as in reference *30* is incorrect. Measurement of the fall velocity in consecutive sections of the fall distance will reveal this possible effect, and is a check on the attainment of terminal velocity.

3. The Faxén wall correction may not be used unrestrictedly with non-Newtonian fluids. It seems to work better in the range of sphere velocities in which non-Newtonian effects are small and also when the ratio of sphere-to-cylinder diameter is small.

4. The zero shear viscosities obtained by the three different extrapolation procedures (Figures 2, 3*a*, 3*b*, and

4) are in reasonably good agreement. One of the extrapolation procedures (Figures 3*a* and 3*b*) is based on the analytical solution for flow past a sphere, and comparison of experimental results with the theory indicates that low enough sphere velocities to estimate $\eta_o$ have been obtained. The extrapolation procedure using a plot of ln $\eta_s$ vs. $(\eta_s v_\infty/D)$, shown in Figure 2, has two rather desirable features. First, it is consistent and straightforward; the same procedure is used with all eight non-Newtonian solutions tested. Second, it permits the use of spheres of different sizes and densities; here the smallest sphere is 0.0635 cm. ruby (density 3.98 g./cc.) and the largest is 0.3175 cm. steel (density 7.76 g./cc.). This is important in precluding complete reliance on only the data with a single set of spheres of the same density. From practical considerations the ability of the plot to incorporate data on spheres of different densities permits the use of the smallest available precision sphere of different materials, since these are usually easier to obtain than precision spheres of progressively smaller diameter of the same material. It should be mentioned that Williams (*30*) used a different extrapolation procedure from the ones presented here. Aside from the uncertainties introduced by his having used a bottom correction unnecessarily and his having had to use unrestrictedly the Faxén correction, since data in only a single cylinder diameter were available to him, the difference is that he plots ln $\eta_s'$ against $(3\eta_s' v_t/D)$, that is, his quantity for the abscissa is three times the value used here. Williams justifies his choice of variable on the grounds that for a Newtonian fluid his $(3\eta_s' v_t/D)$ is the maximum value of the square root of the shear stress tensor. For some of his solutions, moreover, he found it necessary to plot ln $\eta_s'$ against $(3\eta_s' v_t/D)^x$, where the exponent $x$ was adjusted so that the plots fell on straight lines. Obviously, such a procedure, which amounts to a stretching or contracting of the abscissa, is arbitrary. The procedures presented in our paper, based on a large volume of data which account unambiguously for the wall effect, represent a better and more defensible method for estimating $\eta_o$.

5. The drag coefficient correlation, Equation (17), was obtained in terms of the Ellis parameters and with the Faxén wall correction. The parameter $\eta_o$ in the Ellis model was chosen as the value obtained from extrapolation of falling-sphere data. Apparently the Ellis model does not seem to do a good job of describing viscometric data when the parameter $\eta_o$ is chosen as the zero shear viscosity. This is not surprising since, as an empiricism, the model would not be expected to describe the viscometric data over an unlimited range of shear. Because of this, and also the fact that the Faxén correction itself becomes inadequate with non-Newtonian fluids at relatively higher sphere velocities, the correlation works over only the range $(\eta_o v_t/D\tau_{1/2}) \leq 0.3$. In addition, the types of data available do not permit us to account for possible elastic effects which will also become relatively more important at higher sphere velocities.


## ACKNOWLEDGMENT

The author is indebted to Professor R. Byron Bird of the University of Wisconsin under whose supervision this work was done. The financial support of the Wisconsin Alumni Research Foundation, the National Science Foundation (Grants G-11996 and GP-1875), and the American Chemical Society Petroleum Research Fund (Grant 1785-C) is gratefully acknowledged.


## NOTATION

$A, B, C, N$ = dimensionless constants
$D$ = sphere diameter, cm.
$D_c$ = cylinder diameter, cm.
$N_{El} = \eta_o v_t/D\tau_{1/2}$ = Ellis number defined with $v_t$
$F = \frac{1}{6}\pi D^3(\rho_s - \rho)g$ = drag force on sphere, dynes
$F_s = 6\pi\eta_o R v_\infty$ = drag force from Stokes law, dynes
$f = F/\pi R^2 \frac{1}{2}\rho v_t^2$ = drag coefficient for sphere
$f_d$ = wall correction for Newtonian flow past a sphere
$g$ = gravitational acceleration, cm./sec.$^2$
$R = D/2$ = sphere radius, cm.
$N_{Re} = 2Rv_t\rho/\eta_o$ = Reynolds number defined with $v_t$
$v_t$ = measured sphere velocity uncorrected, cm./sec.
$v_\infty$ = sphere velocity corrected for wall effect, cm./sec.

### Greek Letters

$\alpha$ = Ellis model parameter
$\eta$ = non-Newtonian fluid viscosity, poise
$\eta_s = g(\rho_s - \rho)D^2/18v_\infty$ = apparent Stokes viscosity in terms of $v_\infty$, poise
$\eta_s' = g(\rho_s - \rho)D^2/18v_t$ = apparent Stokes viscosity in terms of $v_t$, poise
$\eta_o$ = zero shear viscosity, poise
$\rho$ = fluid density, g./cc.
$\rho_s$ = sphere density, g./cc.
$\tau$ = shear stress, dyne/sq.cm.
$\tau_{1/2}$ = Ellis model parameter, dyne/sq.cm.

## LITERATURE CITED


1. Bacon, L. R., *J. Franklin Inst.*, **221**, 251 (1936).
2. Biery, J. C., and J. D. Huppler, *Univ. Wis. Engr. Expt. Sta. Rept. No. 19* (1962).
3. Caswell, B., and W. H. Schwarz, *J. Fluid Mech.*, **13**, 417 (1962).
4. Chester, W., *J. Fluid Mech.*, **13**, 557 (1962).
5. Faxén, H., *Ark. Mat. Astr. Fys.*, **17**, No. 27, 1 (1922-23).
6. Foster, R. D., and J. C. Slattery, *Appl. Sci. Res.*, **A12**, 213 (1962).
7. Goldstein, S., *Proc. Roy. Soc. (London)*, **A123**, 225 (1929).
8. Happel, John, and Howard Brenner, "Low Reynolds Number Hydrodynamics," Prentice-Hall, Englewood Cliffs, N. J. (1965).
9. Johnson, M. W., Jr., *Phys. Fluids*, **3**, 871 (1960).
10. ———, *Trans. Soc. Rheol.*, **5**, 9 (1961).
11. Ladenburg, R., *Ann. Phys.*, **23**, No. 4, 447 (1907).
12. Lamb, H., "Hydrodynamics," Dover, New York (1945).
13. Langlois, W. E., "Slow Viscous Flow," Macmillan, New York (1964).
14. Leigh, D. C., *Phys. Fluids*, **5**, 501 (1962).
15. Leslie, F. M., *Quart. J. Mech. Appl. Math.*, **14**, 36 (1961).
16. Oseen, C. W., *Ark. Mat. Astr. Fys.*, **6**, No. 29 (1910).
17. Proudman, I., and J. R. A. Pearson, *J. Fluid Mech.*, **2**, 237 (1957).
18. Rathna, S. L., *Quart. J. Mech. Appl. Math.*, **15**, 427 (1962).
19. Reiner, M., "Deformation, Strain and Flow," Interscience, New York (1960).
20. Sato, T., I. Taniyama, and S. Shimokawa, *Kagaku Kogaku*, **30**, 34 (1966).
21. Slattery, J. C., *A.I.Ch.E. J.*, **8**, 663 (1962).
22. ———, Ph.D. thesis, Univ. Wisconsin, Madison (1959).
23. ———, and R. B. Bird, *Chem. Eng. Sci.*, **16**, 231 (1961).
24. Tanner, R. I., *J. Fluid Mech.*, **17**, 161 (1963).
25. ———, *Chem. Eng. Sci.*, **19**, 349 (1964).
26. Tomita, Y., *Bull. Jap. Soc. Mech. Engr.*, **2**, No. 7, 469 (1959).
27. Turian, R. M., Ph.D. thesis, Univ. Wisconsin, Madison (1964).
28. Valentik, L., and R. L. Whitmore, *Brit. J. Appl. Phys.*, **16**, 1197 (1965).
29. Wasserman, M. L., and J. C. Slattery, *A.I.Ch.E. J.*, **10**, 383 (1964).
30. Williams, M. C., *ibid.*, **11**, 467 (1965).
31. Ziegenhagen, A. J., R. B. Bird, and M. W. Johnson, Jr., *Trans. Soc. Rheol.*, **5**, 47 (1961).
32. Ziegenhagen, A. J., *Appl. Sci. Res.*, **14**, 43 (1965).



*Manuscript received May 23, 1966; revision received February 24, 1967; paper accepted February 24, 1967.*